



EVALUATION OF RUPTURE DIRECTIVITY EFFECTS ON STRONG GROUND MOTION BASED ON HYBRID SIMULATION METHOD

Hongjun SI¹ and Saburoh MIDORIKAWA²

SUMMARY

The effect of rupture directivity on pseudo velocity response spectra is evaluated by ground motion simulation based on the hybrid simulation method. In order to examine the influence of the rupture directivity on attenuation relationships, a directivity effect factor D is introduced, which is the ratio of the amplitude of the simulated motion to the average amplitude of the attenuation relation. The results indicate that, for earthquakes with unilateral faulting, there are strong directivity effects on pseudo velocity response spectra, especially for those with the periods longer than 0.5 sec. A comparison of the results with the observed records of the 1979 Imperial Valley earthquake shows that the simulated directivity effect factor D well matches the observed one. The distribution of the D value is represented by simple functions. By using the factor, the pseudo velocity response spectra predicted by an attenuation relationship can be corrected considering the rupture directivity effects.

INTRODUCTION

The results from recent studies indicate that the rupture directivity effects should be considered in the prediction of ground motion. Somerville et al. [1] discovered the directivity effects on spectral amplitudes at periods longer than 0.6 sec, and they proposed the modification factors to empirically take into account of the rupture directivity effects. Some evidences that support the existence of directivity effects at shorter periods has also been obtained. Boatwright and Boore [2] and Midorikawa [3] reported the strong directivity effects on peak ground accelerations of both the 1980 Livermore valley earthquake and the 1985 Chile earthquake respectively. By numerical simulation of high-frequency ground motions, Archuleta and Hartzell [4] also revealed the strong directivity effects on near-source ground accelerations. These results suggest that the directivity effects should be considered in the attenuation relationship.

Due to the limitation of observed data, it is, at the present impractical to derive general rule on the directivity effects from the records. Consequently, an analytical approach was suggested [5]. Over the past years, we have simulated the strong ground motion with the stochastic Green's function method, and evaluated the effect of rupture directivity on both peak acceleration and peak velocity. In this paper, the

¹ Ph.D, Kozo Keikaku Engineering Inc., Japan, Email: shj@kke.co.jp

² Professor, Tokyo Institute of Technology, Japan, Email: smidorik@enveng.titech.ac.jp

effects of the rupture directivity on pseudo velocity response spectra are evaluated on the basis of the hybrid method of ground motion simulation.

METHODOLOGY

Hybrid method of ground motion simulation

In order to evaluate the effect of rupture directivity on the pseudo velocity response spectra, the hybrid simulation technique is employed in this study. This method is identical to that used by Irikura and Kamae [6] and has been proven to be very effective to simulate the broadband ground motions from large earthquakes.

The earth media is idealized as a stratified half space model. The discrete-wave number/finite-element technique (DWFE) [7], extended to finite-fault source characterization [8][9], was used to determine low-frequency seismograms, and the stochastic Green's function method [10] was used to calculate high-frequency seismograms. With respect to the stochastic Green's function method, the synthetic motions are calculated by using the empirical Green's function method proposed by Irikura [11] in which small event motions are calculated with the stochastic simulation method suggested by Boore [12]. The radiation pattern in the stochastic Green's function method is represented by using the frequency dependent scheme described by Irikura and Kamae [13].

In the simulation, the matching filter for combining the low and high frequency motion is a linear one, by which the lower frequency motions decrease from a period of 2.0 sec to 1.0 sec, while the high frequency increase from 1.0 sec to 2.0 sec.

In order to avoid the bias caused by the stochastic source function generated from a white noise time series, the simulation were conducted ten times, and their average of the 5% damped pseudo velocity response spectra are determined for the consequent analysis by using the ten synthetic waveforms.

For conciseness, we refer to the 5% damped pseudo velocity response spectra as PSV hereafter.

Method for evaluating the effect of rupture directivity on ground motion

For evaluating the influence of rupture directivity on attenuation relationships, the directivity effect factor D was introduced, which is the logarithm of the ratio of the simulated PSV [${}_vS(T)$] of fault normal component to the reference PSV as shown in Eq. (1). Here, the reference PSV will be calculated from an attenuation relation derived from the resultant PSV of the synthetic horizontal components.

$$D = \log ({}_vS(T)_{\text{simulated}} / {}_vS(T)_{\text{reference}}) \quad (1)$$

THE SIMULATION OF GROUND MOTIONS

Fault model and station configuration

The synthetic seismograms for an M7.0 earthquake was calculated with a pure strike-slip mechanism and a seismic moment M_0 3.98×10^{19} Nm. Fig. 1 illustrates the fault model used to simulate broad band ground motions at stations regularly distributed around the fault. There is only one asperity on the fault model, designed just like the fault model of the 1979 Imperial Valley, California earthquake. The table 1 shows the fault parameters used in the analysis.

The fault is 2 km deep under the ground surface with its length and width of 30 km and 13 km, respectively. Its location and the station configuration are shown in Fig. 2. A rupture velocity of 2.52 km/sec and an exponential source-time function with duration of 1.5 sec were used in the analysis. The

asperity area was divided into 10×8 subfaults with each fault having an area of $1.0 \times 1.0 \text{ km}^2$, seismic moment M_0 of $2.45 \times 10^{16} \text{ Nm}$. The back ground area are divided into 115 subfaults with each having an area of $2.0 \times 1.0 \text{ km}^2$ and seismic moment M_0 of $8.15 \times 10^{15} \text{ N m}$. The number of subfaults was determined on basis of the scaling relationship.

Table 1 Fault parameters

Strike, Dip	270.0°, 90.0°	
M_w	7.0	
M_0	3.98E+19 Nm	
Length, Width	30km, 13km	
Fault depth	2km	
D	310.0cm	
$\Delta\sigma$	3.00MPa	
V_r	2.52km/s	
F_{max}	8.5Hz	
μ	3.3E+10 N/m ²	
Rise time	1.5s	
	Asperity	Back ground
M_{0a}	1.76E+19Nm	2.22E+19Nm
S_a	85.8 km ²	304.2km ²
D_a	623.1cm	221.2cm
$\Delta\sigma_a$	13.6MPa	2.7MPa

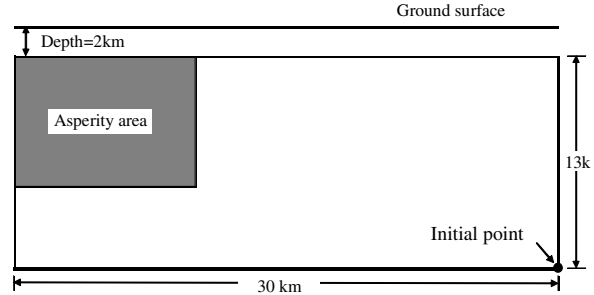


Fig. 1 Asperity source model with back ground assumed for the simulation

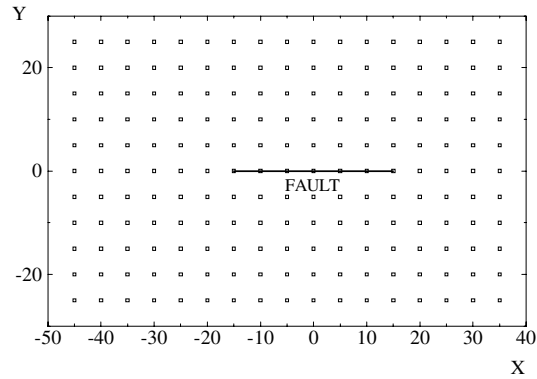


Fig. 2 Fault location and the station configuration

Earth model

The earth model used in the analysis consists of 6 uniform layers overlying a half-space containing the fault. The profile of the model including the velocity of P, S wave and density are shown in Table 2. The amplification factor for the high frequency motion, with a predominant period of about 2 sec, is calculated using the layers above the bedrock layer with a shear wave velocity of 3.0 km/sec, and the low frequency motion are calculated by using all the layers described in table 2.

Table 2 The earth model used in the analysis

No.	Density (g/cm ³)	V_p (km/s)	V_s (km/s)	Q-Value	H (km)
1	2.2	2.10	0.60	50	0.022
2	2.4	2.60	0.80	100	0.058
3	2.6	3.70	1.20	100	0.080
4	2.6	4.65	1.80	150	0.340
5	2.6	5.50	3.00	200	1.500
6	2.7	6.05	3.50	270	14.000
7	2.8	6.60	3.80	400	-

RESULTS AND DISCUSSION

Synthetic waveforms

The simulated velocity waveforms are shown in Figs. 3 and 4 for faults parallel and normal components, respectively. The waveforms are integrated from the synthetic acceleration waveforms.

From the figures 3 and 4, it can be seen that the effect of rupture directivity on the synthetic waveforms of the fault normal components is significant. Hence, only the fault normal components are taken into account in this study for the evaluation of the rupture directivity effects on pseudo velocity response spectra.

The attenuation relation for estimation of the reference PSV

The attenuation relation model for determines the reference PSV in Eq. (1) is shown in Eq. (2).

$$\log {}_vS(T) = a(T) - \log(X+c) - k(T) X \quad (2)$$

Where ${}_vS(h, T)$ is the 5% damped PSV, and X is the closest distance to the fault plane.

In Eq. (2), the coefficient c was taken as 6 km over all periods. The coefficient $a(T)$ and $k(T)$ are determined by fitting the equation to the resultant PSV of the synthetic horizontal components. The fitting curves and the data at periods 0.1, 0.5, 1.0 and 2.0 sec are shown in Fig. 5, respectively, which stands for the average of the synthetic PSVs.

Distribution of the rupture directivity effect factor, the D value

The simulated distribution of D value is shown in Figs. 6 for PSV at period $T=0.1, 0.5, 1.0,$ and 2.0 sec, respectively. In the figure 6, the red line represents the fault plane's projection to surface. The star stands for the epicenter. The center of the fault is located at the origin point of the coordinate system (x, y) in the figures. The color shows the quantity of the D value.

In Figure 6, the following characteristics of the spatial distribution of the D values can be observed.

- (1) For $T=0.1$ sec, the D value is positive and in the forward direction of the rupture propagation. This shows that the strong motion is greater than the average one. The D values in the area out of the edge of the fault have a range from 0.03 to 0.15. The D value doesn't depend upon the angle between the direction of the fault strike and that from the epicenter to a station. In the backward direction, the D values are negative, which shows that the strong motion is less than the average one.
- (2) For $T=0.5, 1.0$ and 2.0 sec, the D value varies with the angle between the direction of the fault strike and that from the epicenter to a station. At the periods of $T=0.5, 1.0$ and 2.0 sec, the maximum D values are equal to about 0.3, 0.4 and 0.7 respectively, in the area about 15 km from the fault.

For the purpose of quantitative analysis of the spatial distribution of the D values, the cross-section on the fault for $T=0.1, 0.5, 1.0, 2.0$ and 5.0 sec are shown in Fig. 7(a), which indicates that the D value increases within and near the fault zone along the forward rupture direction from the epicenter. Its maximum values, as described in (2), almost appear in the area about 15 km away from the fault edge for all periods. The D value for the longer periods is generally greater than those for at the shorter periods. At 5.0 sec, however, the D value become smaller for $T=2.0$ sec, which implies the possible influence of the site effects.

Fig. 7(b) shows the D value for $T=1.0$ and 2.0 sec on the cross-section perpendicular to the fault with $X=-15.0$ km. The figure shows that the distribution of D value can be approximated by a cosine function, with a maximum at the center.

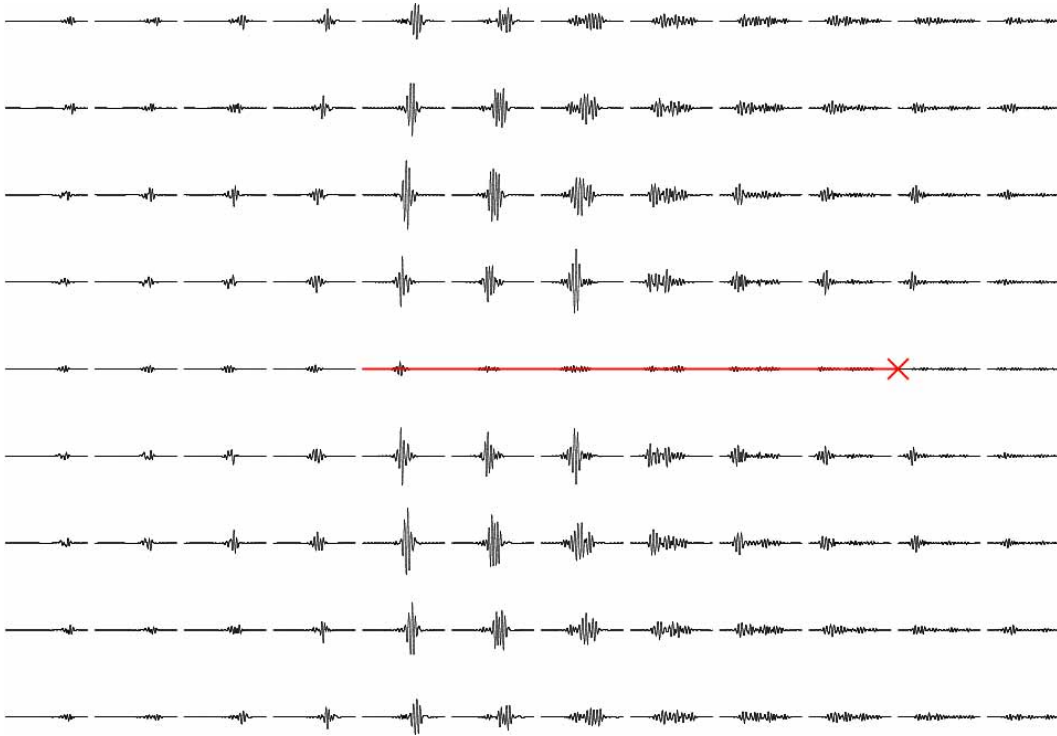


Fig. 3 Fault parallel components of the synthetic waveforms

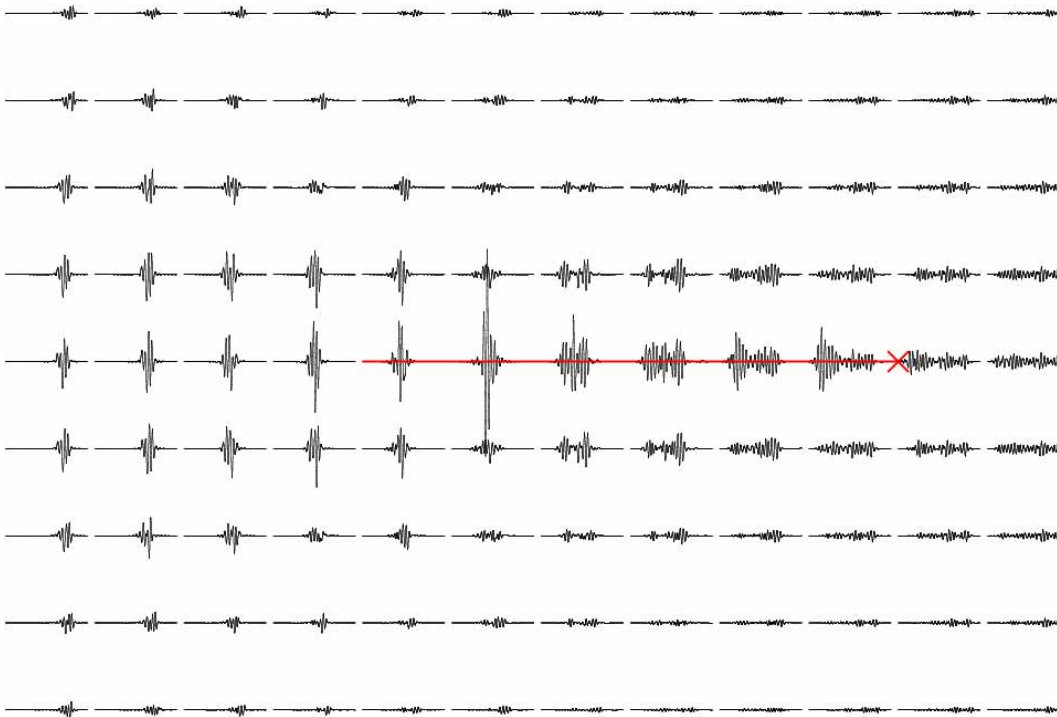


Fig. 4 Fault normal components of the synthetic waveforms

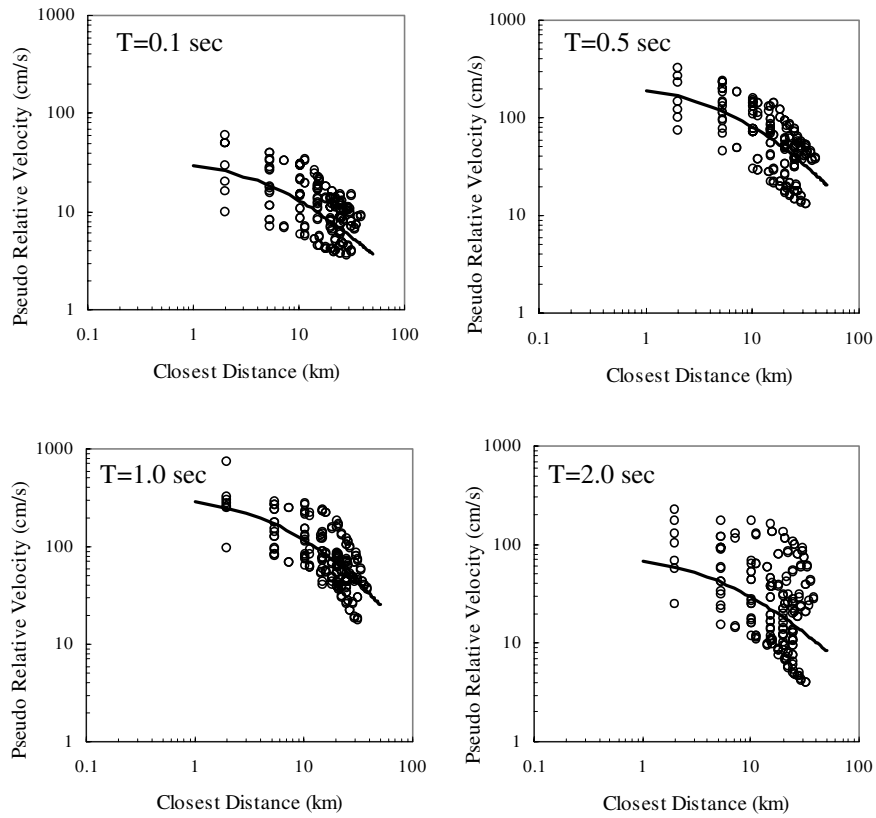


Fig. 5 Simulated PSV and the reference PSV

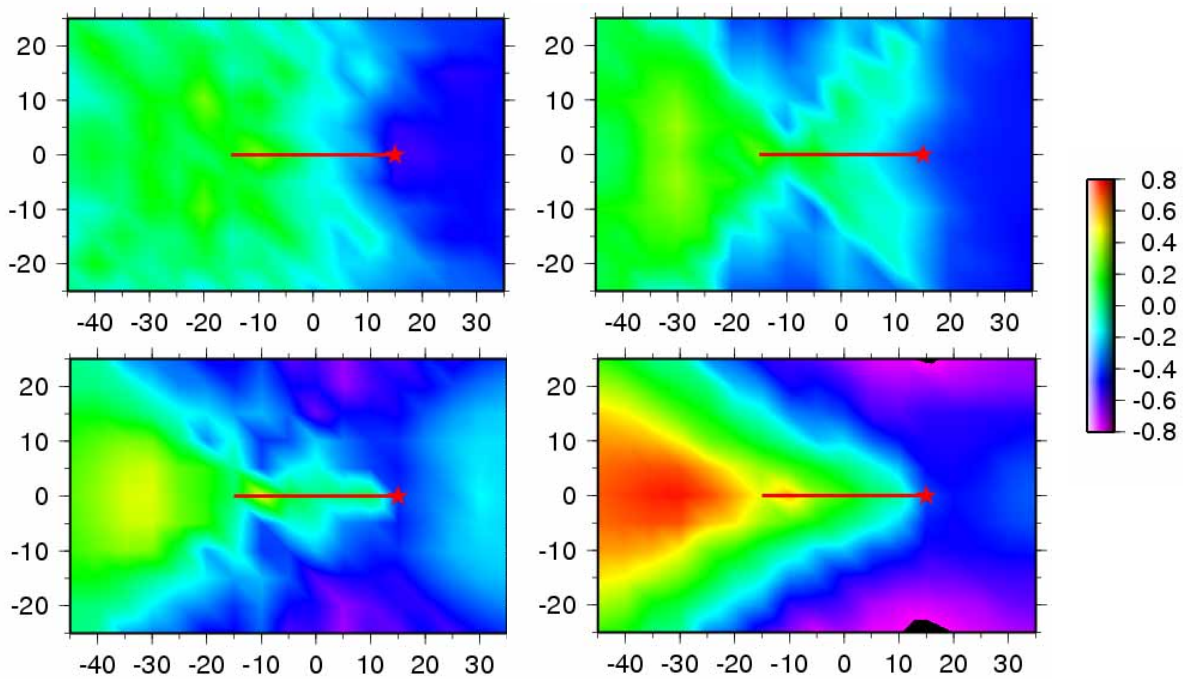


Fig. 6 Distribution of the directivity effect factor, D
 (Upper: left: $T=0.1$ sec, right: $T=0.5$ sec; Lower: left: $T=1.0$ sec, right: $T=2.0$ sec)

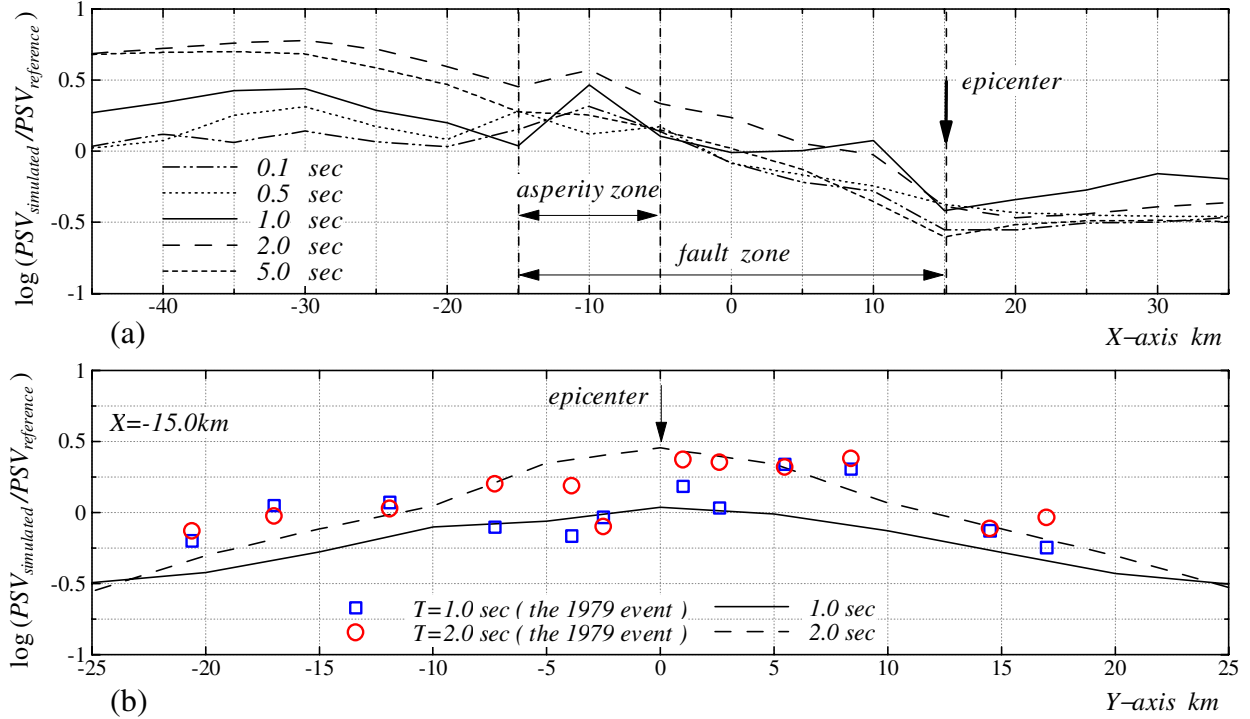


Fig. 7 Distribution of the D value on the cross sections

Comparison with the records during the 1979 Imperial Valley, California, earthquake

We selected 18 fault normal records observed during the 1979 Imperial Valley, California, earthquake [M_w 6.5, M_0 $5\text{-}7 \times 10^{18}$ Nm], under the criterion that the shear-wave velocity averaged over the upper 30 m at the station and the record is available. Fig. 8 shows the map of the selected stations, and the location of the rupture fault.

In order to determine the D value for the seismic records, the reference PSV defined in Eq. (1) is calculated by using the attenuation relation proposed by Boore et al. [14], in which the site effects is evaluated in terms of the average shear-wave velocity to 30 m. Figs. 9 show the PSV calculated by Boore et al. [14] and that observed during the earthquake.

Since there are 12 stations located on the cross section perpendicular to the fault at the fault edge, the D value for the 12 stations were plotted in Fig. 7(b) for T=1.0 and 2.0 sec. The figure shows that the D value calculated from the observed records is consistent with the simulated D value, especially for T=2.0 sec, and for T=1.0 sec in the range from Y=-10.0 to 10.0 km. For T=1.0, the observed D values are greater than that simulated except the area from Y=-10.0 to 10.0 km. This may be caused by the difference between the reference PSVs used in the Eq. (1).

Modeling of the spatial distribution of the D value

For the purpose of developing the modification factor to include the directivity effect in the attenuation relationship, the D values are preferable to be represented by a simple function. To do this, we follow two steps. Firstly, the variation of the D value along the fault (when Y=0 km), as shown in Figs. 7(a), is fit with the function C. Secondly, the function S is introduced to represent the variation of the D value along the Y-coordinate. As a result, D is expressed by Eq. (3):

$$D=C \times S \quad (3)$$

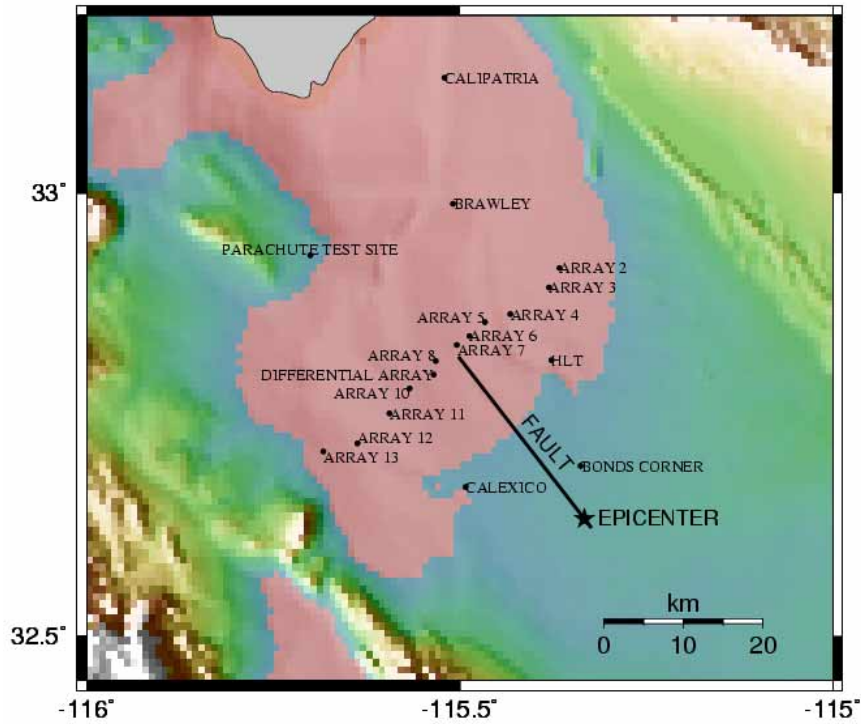


Fig. 8 Observation stations and rupture fault of the 1979 Imperial Valley earthquake

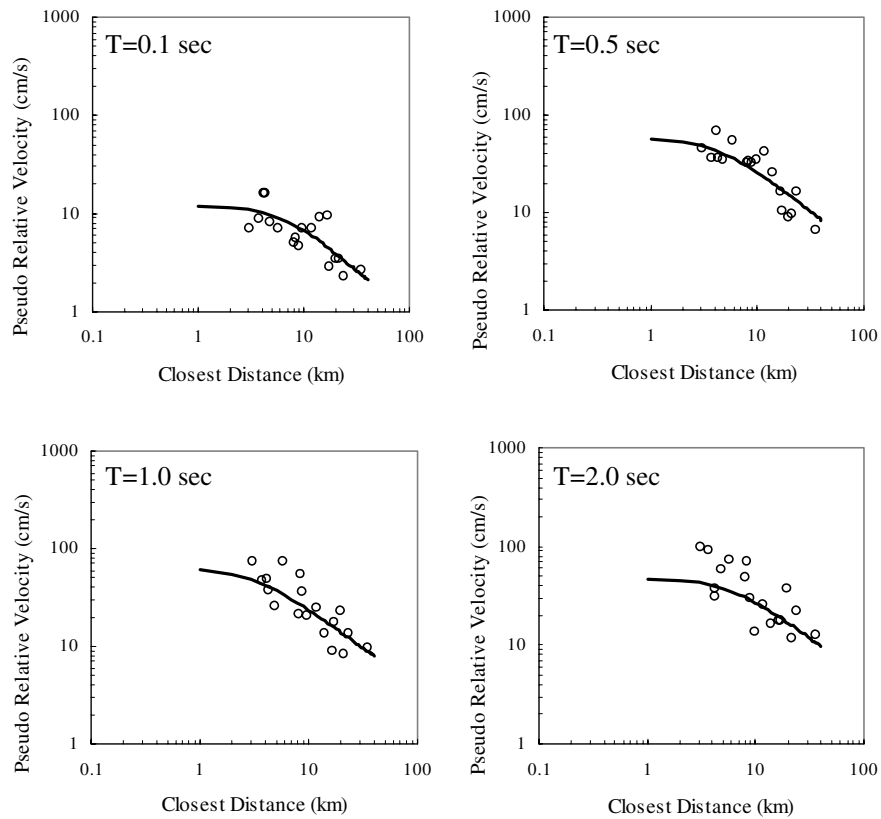


Fig. 9 The observed PSV data and the attenuation equation by Boore et al. [14]

As shown in Fig. 7(a), the D value for the period value less than 0.5 sec, near 1.0 sec, and greater than 2.0 sec are generally similar to each other, for the simplicity, the C functions are classified to the 3 categories above. The C functions are derived in the forms shown as Eq. (4) – (6), and illustrated in Fig. 10 (red lines).

$$C = 0.30\cos(-4.6x/3L-1.5)-0.15 \quad (40.0 \text{ km} \leq x \leq X_{ec}, T \text{ shorter than } 0.5 \text{ sec}) \quad (4)$$

$$C = 0.30\cos(-4.6x/3L-1.5) \quad (40.0 \text{ km} \leq x \leq X_{ec}, T \text{ near or equal } 1.0 \text{ sec}) \quad (5)$$

$$C = 0.70\cos(-4.6x/3L-1.7) \quad (40.0 \text{ km} \leq x \leq X_{ec}, T \text{ longer than } 2.0 \text{ sec}) \quad (6)$$

Where, L is the length of the fault, taken into account according to Somerville et al. [1], and X_{ec} is the coordinate of the epicenter.

In order to represent the variation of the D value along the y-coordinate, we introduce the parameter θ , which is defined in Fig. 11. The S function is in the form as shown in Eq. (7)

$$S = 1 \quad (\theta \leq 45; T < 0.5 \text{ sec}) \quad (7)$$

$$= |\cos\theta| \quad (\theta \leq 45; T \geq 0.5 \text{ sec})$$

As a reference, the modification models proposed by Somerville et al. [1] were also shown in Fig. 10. Because the definition of the D value in Somerville et al. [1], i.e., the ratio of the average horizontal response spectral acceleration with respect to an attenuation equation, is different from what was defined in this paper, a direct quantitative comparison was not done. But it can be say that, the general tendency of their results are consistent with ours.

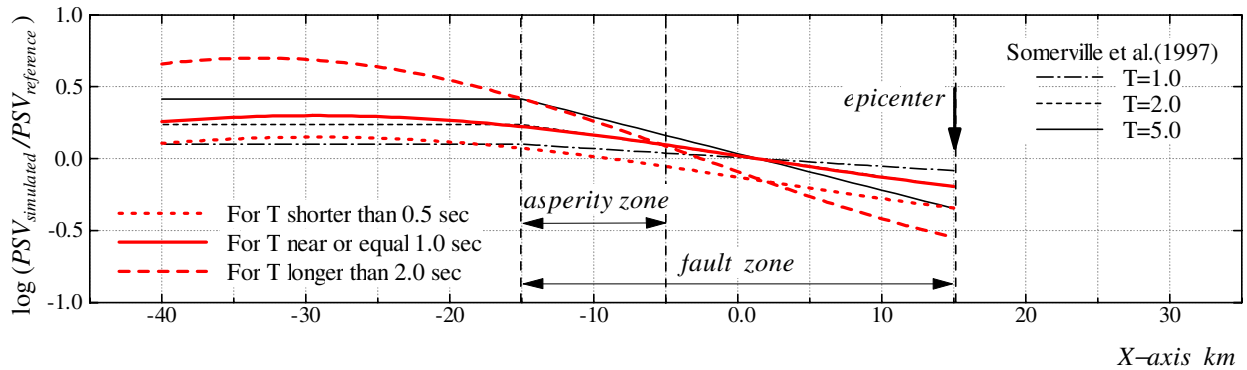


Fig. 10 The C functions defined in Eq. (4) - (6)

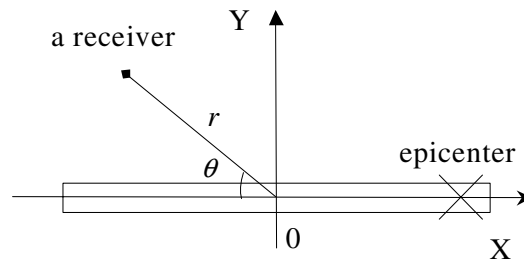


Fig. 11 Definition of θ

CONCLUSIONS

The effect of rupture directivity on pseudo velocity response spectra is evaluated by ground motion simulation based on the hybrid simulation method. In order to examine the influence of the rupture directivity on attenuation relationships, a directivity effect factor D is introduced, which is the ratio of the amplitude of the simulated motion to the average amplitude of the attenuation relation. The results indicate that, for earthquakes with unilateral faulting, there are strong directivity effects on pseudo velocity response spectra, especially for those with the periods longer than 0.5 sec. A comparison of the results with the observed records of the 1979 Imperial Valley earthquake shows that the simulated directivity effect factor D well matches the observed one. On the other hand, because there are no sufficient strong motion data in the far field, the simulated D value in the far field still remains unchecked by the records during an earthquake.

The distribution of D value is represented by simple functions. By using the factor D , the pseudo velocity response spectra predicted by an attenuation relationship can be corrected considering the directivity effects.

ACKNOWLEDGEMENTS

A number of figures were made using GMT (Wessel and Smith, 1991). The strong motion data from the 1979 Imperial Valley earthquake used in the analysis are provided by National Geographical Data Center (Earthquake Strong Motion CD-ROM, 1996).

REFERENCES

1. Somerville PG, Smith NF, Graves RW, Abrahamson NA. "Abrahamson. Modification of empirical strong ground motion attenuation relations to include the amplitude and duration effects of rupture directivity". *Seism. Res. Lett.* 1997; 68: 199-222.
2. Midorikawa S. "Attenuation of the peak ground acceleration and velocity during the 1985 Chile and Nihonkai-chubu earthquakes". *Journal of Struct. Construct. Eng.* 1991; 422: 37-44 (in Japanese, with English abstract).
3. Boatwright J, Boore DM. "Analysis of the ground accelerations radiated by the 1980 Livermore Valley earthquakes for directivity and dynamic source characteristics". *Bull. Seism. Soc. Am.* 1982; 72: 1843-1865.
4. Archuleta RJ, Hartzell SH. "Effects of fault finiteness on near-source ground motion". *Bull. Seism. Soc. Am.* 1981; 71: 939-957.
5. SI H, Midorikawa S. "Evaluation of rupture directivity effects on peak ground motion using stochastic Green's function method". *Journal of Struct. Construct. Eng.* 2001; 546: 47-53 (in Japanese, with English abstract).
6. Irikura K, Kamae K. "Strong ground motions during the 1948 Fukui earthquake –Estimation fo broad-band ground motion using a hybrid simulation technique-". *Zisin* 1999; 52(1): 129-150 (in Japanese, with English abstract).
7. Olson AH, Orcutt JA, Frazier GA, "The discrete wave number/finite element method for synthetic seismograms". *Geophys. J. R. Astr. Soc.* 1984; 77: 421-460.
8. Spudich, P, Archuleta R, "Techniques for earthquake ground motion calculation with applications to source parameterization of finite faults", Bolt BA editor. *Seismic strong motion synthetics: Orlando, Florida: Academic Press, 1987: 205-265.*
9. Spudich, P, Xu L. "Software for calculating earthquake ground motions from finite faults in vertically varying media". Lee WHK, Kanamori H, Jennings P, Kisslinger C, editors.

- International handbook of earthquake and engineering seismology, Volume 2. Orlando: Academic Press, 2002.
10. Kamae K, Irikura K, Fukuchi Y. "Prediction of strong ground motion based on scaling law of earthquake". Journal of Struct. Construct. Eng. 1991; 430: 1-9 (in Japanese, with English abstract).
 11. Irikura, K. "Prediction of strong acceleration motions using Green's function". Proc. 7th Japan Earthquake Engineering Symp. 151-156, 1986.
 12. Boore DM. "Stochastic simulation of high frequency ground motion base on seismological models and radiated spectra", Bull. Seism. Soc. Am. 1983; 73: 1865-1894.
 13. Irikura K, Kamae K. "Estimation of strong motion in broad-frequency band based on a seismic source scaling models and an empirical Green's function technique". ANNALI DI GEOFISICA, XXXVII, 1994; 6: 1721-1743.
 14. Boore DM, Joyner WB, Fumal TE. "Equations for estimating horizontal response spectra and peak acceleration from western North American earthquakes: A summary of recent work". Seism. Res. Lett. 1997; 68: 128-151.